PNC-TN9410 89-078

SUBCHANNEL ANALYSIS BY THE FIDAS CODE BASED ON THE THREE-FLUID MODEL

May, 1989

OARAI ENGINEERING CENTER
POWER REACTOR AND NUCLEAR FUEL DEVELOPMENT CORPORATION

複製又はこの資料の入手については，下記にお問い合わせください。
〒311-13　茨城県東茨城郡大洗町成田町4002
動力炉・核燃料開発事業団
大洗工学センター　システム開発推進部・技術管理室

Enquires about copyright and reproduction should be addressed to: Technology Management Section O-arai Engineering Center, Power Reactor and Nuclear Fuel Development Corporation 4002 Narita-cho, O-arai-machi, Higashi-Ibaraki, Ibaraki-ken, 311-13, Japan

動力炉・核燃料開発事業団（Power Reactor and Nuclear Fuel Development Corporation）

PNC-TN9410 89-078
May 1989

SUBCHANNEL ANALYSIS BY THE FIDAS CODE BASED ON THE THREE-FLUID MODEL(*)

Satoru Sugawara[1], T. Sakai[1], K. Watanabe[2] and H.E.C. Rummens[3]

ABSTRACT

The Film Dryout Analysis Code in Subchannels, FIDAS, has been developed with the main objective of predicting dryout and post-dryout heat transfer in channels and in rod bundles. In FIDAS, two-phase flow consisting of continuous liquid film, continuous vapor and entrained droplets is modeled by a three-fluid, three-field representation of 12 field equations, i.e. three continuity, three energy and six momentum equations. In this validation study of the code, inter-subchannel mixing models were examined. FIDAS satisfactorily predicted flow quality and mass flux in subchannels under typical operating conditions of a boiling water reactor, as comparisons with the experimental data of GE 3x3 and ISPRA 4x4 tests.

---

[1] O-arai Engineering Center, Power Reactor and Nuclear Fuel Development Corporation, O-arai, Ibaraki, 311-13 Japan

[2] Nuclear Data Corporation, 1-1-71 Nakameguro, Meguro, Tokyo, 153 Japan

[3] work while at PNC, on leave May-Nov 1988 from Dept. of Eng. Physics, McMaster University, Hamilton, Ontario, L8S 4M1 present affiliation ; Chalk River Nuclear Laboratories, Chalk River, Ontario, K0J 1J0 Canada

(*) to be presented to the Fourth International Topical Meeting on Nuclear Reactor Thermal-Hydraulics (NURETH-4), October 10-13, 1989, Karsruhe F.R.G.

CONTENTS

LIST OF TABLES

LIST OF FIGURES

1. INTRODUCTION

Prediction of dryout occurrence and estimation of post-dryout temperature behavior of fuel cladding in rod bundles are of primary concern in water-cooled nuclear reactor design and safety evaluations. A number of full-scale mockup tests have been carried out so far to obtain experimental data on the dryout and post-dryout heat transfer. Empirical correlations have been developed from these accumulated dryout and post-dryout data and have been widely applied to design and safety evaluations. However, a result of this situation is that the empirical correlations are restricted to ranges within experimental conditions.

One of the possible approaches in resolving this issue is subchannel analysis, to treat the dryout phenomenon and post-dryout heat transfer on the basis of multi-fluid modeling coupled with an annular flow film dryout criterion.

In subchannel analysis, a matter of great account is inter-subchannel mixing including the 'void drift' phenomenon. In the analysis of inter-subchannel mixing, empirical correlations in which mixing rates are calculated as a function of axial flow velocity have been so far applied. Obviously, it is necessary to introduce more theoretical models to describe complex phenomena such as two-phase inter-subchannel mixing in rod bundles. The theoretical approach should be based on the mixing length and/or eddy diffusivity, or Reynolds stress model.

The resulting sophisticated analytical model is based on a multi-fluid approach in which phasic conservation equations are used.[1] Such an approach has been adopted by state-of-the-art computer codes (eg. THERMIT-II[2], COBRA-TF[3]). Unfortunately, there remains considerable uncertainty in the proper formulation of interfacial transfer laws.

Therefore, the Film Dryout Analysis Code in Subchannels (FIDAS) has been developed by the author in the Power Reactor and Nuclear Fuel Development Corporation (PNC), with the main objective of predicting the dryout and post-dryout heat transfer in channels and in rod bundles. The interfacial mass transfer

models for droplet entrainment and deposition were developed and included in the code to provide more accurate film dryout analysis capability.[4] Moreover, validation studies of the developed code and models have been performed against experiments conducted over a wide range of conditions in the water-cooled reactor environment.[5][6]

In this paper, an outline of the FIDAS code is described and the inter-subchannel mixing models are validated by comparisons with the experiments of GE[7] and ISPRA[8] in which subchannel flow and enthalpy distributions have been measured.

2. THE FIDAS FORMULATION AND CALCULATIONAL FEATURE

The three-fluid/three-field model is considered to be most appropriate to provide the capability of describing film dryout phenomenon, thermal non-equilibrium effect and inter-subchannel mixing. Therefore, FIDAS provides a three-fluid, three-field representation of two-phase flow in a channel or rod bundles as shown in Fig.1. The three fields are specified by continuous liquid film, continuous vapor and entrained liquid droplets suspended in vapor. Thus a set of basic 12 field equations given in Table 1 is built into the code, namely three continuity, three energy, and six momentum equations. The 12 field equations together with the volume fraction conservation relation among three fields enable us to obtain analytical information for the following 13 parameters: three axial and three lateral velocities, three volume fractions, three specific enthalpies, and pressure.

The central feature of the code is its ability to simulate the dryout phenomenon at the heated wall. In order to predict the dryout occurrence and post-dryout temperature behavior of a heated surface, the code provides the capability to simulate flow regime evolution in subchannels as shown in Fig.2; i.e. single-phase liquid flow at the entrance, bubbly/slug flow formulation by evaporation, transition to a liquid-vapor-droplet annular flow, a further transition to vapor-droplet mist flow due to liquid film disappearance from the heated surface, and

superheated single-phase vapor flow formulation due to complete evaporation of all droplets. In this evolution process, the onset of dryout is defined as the disappearance of liquid film adhering to the heated surface.

The computational scheme of the code is constructed on the basis of a semi-implicit method. The Skyline solver is used to solve the linear finite-difference matrix which is derived from the basic 12 finite-difference equations by linearizing by means of Taylor's expansion. The specifications for boundary conditions are the inlet velocity (or mass flux), inlet temperature (or enthalpy), heat flux to the wall, and the outlet pressure. A staggered mesh is used, and the time step is adjusted according to velocity limits (expressed by the Courant number) and diffusion limits.

3. PHYSICAL MODELS AND CONSTITUTIVE EQUATIONS

The following constitutive equations are provided in the code:

(a) Droplet entrainment rate.
(b) Droplet deposition rate.
(c) Wall shear stress, between wall and liquid film in the pre-dryout region, and between wall and vapor in the post-dryout region.
(d) Vapor-liquid and vapor-droplet interfacial drag forces.
(e) Droplet size.
(f) Convective heat transfer, between wall and liquid film in the pre-dryout region, between wall and vapor in the post-dryout region, and between wall and droplet in the post-dryout region.
(g) Radiative heat transfer, between wall and vapor, and wall and droplet.
(h) Vapor-liquid and vapor-droplet interfacial heat transfer.
(i) Interfacial mass transfer, by condensation and vaporization.
(j) Criteria of flow regime transition to annular flow.

The field and principal constitutive equations used in the present study are summarized in Tables 1 and 2. The droplet

entrainment and deposition models used have been validated in previous study[4]. The interfacial shear stress between liquid film and vapor is estimated by the well-known Wallis correlation; the wall shear stress and drag force of droplet are given by conventional single phase correlations. The average droplet diameter is determined from the critical Weber number. The transition to annular flow is estimated by a formula obtained from the slug/annular transition boundary in the well-known Baker flow regime diagram.

The conservation equations, as well as the constitutive relations for various models, are described in detail in Ref.[4].

4. INTER-SUBCHANNEL MIXING MODEL

4.1 Theory

The exchange or mixing of coolant between adjacent subchannels is one of the most important phenomena that must be accounted for in subchannel analysis, since it leads to the transfer of mass, energy and momentum between adjacent subchannels. This mixing can be classified as two types, forced or natural. Forced mixing is caused by mechanical obstructions, such as spacer grids or wire wrap. On the other hand, natural mixing consists of turbulent mixing and diversion cross flow. Turbulent mixing results from the natural eddy transport between subchannels, while diversion cross flow is caused by lateral pressure gradients.

An additional mixing phenomenon, known as 'void drift', has been postulated to occur in two-phase flows. In experimental observations, vapor tended to diffuse toward unobstructed regions.[7] This cannot be predicted using turbulent mixing alone. Hence, the void drift effect must be included as a separate type of natural mixing in two-phase flows. This type of mixing is assumed to be dominant in the bubbly and/or slug flow regime[7], while turbulent mixing exists in all flow regimes.

If all these types of mixing are present, then they must be accounted for in the analytical model. Therefore, in FIDAS,

these have been considered except the forced mixing, since the use of wire-wrap or flow diverters is not common in the rod bundles of light water cooled reactor. The mixing models applied to each flow regime are summarized in Fig.2. As shown in the figure, the diversion cross flow and the turbulent mixing are applied to all flow regimes, while the void drift effect is considered in only the bubbly and slug flow regimes.

(1) Diversion Cross Flow

Diversion cross flow can be obtained from the force balance of the lateral pressure gradient and the lateral friction force at the wall-fluid and fluid-fluid interfaces. The lateral friction force is calculated using constitutive equations listed in Table 2.

(2) Turbulent Mixing

Turbulent mixing can be calculated by Prandtl's mixing length theory. From this theory, mixing terms for the mass, energy and momentum equation are expressed as follows:

$$w_{ij} = -(\varepsilon_M + \varepsilon_M^T)\nabla \rho_{ij} = -\left(\frac{\mu}{\rho\, Sc} + \frac{\mu^T}{\rho\, Sc^T}\right)\nabla \rho_{ij} , \quad (1)$$

$$q_{ij} = -(\varepsilon_E + \varepsilon_E^T)\nabla (\rho h)_{ij} = -\left(\frac{\mu}{\rho\, Pr} + \frac{\mu^T}{\rho\, Pr^T}\right)\nabla (\rho h)_{ij}, \quad (2)$$

$$\tau_{ij} = -(\varepsilon_u + \varepsilon_u^T)\nabla (\rho u)_{ij} = -\left(\frac{\mu}{\rho} + \frac{\mu^T}{\rho}\right) \nabla (\rho u)_{ij}, \quad (3)$$

with,

$$\mu^T = \rho\ l_m^2 \sqrt{\Sigma \left(\frac{\partial u}{\partial L} + \frac{\partial v}{\partial X}\right)^2} , \quad (4)$$

where ε is the diffusion coefficient and l_m is the mixing length. The subscripts i and j are subchannel numbers, and X and L denote the axial and lateral directions. The superscript T stands for turbulent property. These terms are computed only for the continuous phase. The continuous phase is assumed to be liquid phase in the bubbly flow, and vapor and liquid film in the

annular flow. Linear interpolation is used in the intermediate region. The mixing length, l_m is expressed as follows:

$$l_m = K_1 D_{h,ave} = K_1 \left(\frac{D_{h,i} + D_{h,j}}{2}\right) . \quad (5)$$

where K_1 is an experimentally determined value from the available data.

(3) Void Drift Model

The mixing term used for the void drift phenomenon is as follows:

$$\phi_{ij} = (\varepsilon / l_m)_2 \phi \left[- \nabla (\Omega \phi)_{ij,FD} \right] , \quad (6)$$

where ϕ_{ij} represents the generalized mixing term, Ω stands for the mass, energy or momentum equation, and ϕ denotes ϕ phase. In the mass equations, ϕ_{ij} represents an additional mass exchange rate between adjacent subchannels. In the energy equations this term represents the apparent heat flux at channel boundaries. Finally, in the momentum equations, it is an apparent shear stress acting along channel boundaries.

In equation(6), the subscript FD denotes fully-developed distribution. The assumption used by Lahey[7] is also used as a basis for developing expressions; it states that the fully-developed void fraction distribution is proportional to the fully-developed mass velocity distribution. From this assumption, the following equation is obtained:

$$\nabla (\Omega \phi)_{ij,FD} = K_2 \frac{(G_i - G_j)}{(G_i + G_j)} \nabla (\Omega \phi)_{ij} , \quad (7)$$

where K_2 is an experimentally determined value.

$(\varepsilon / l_m)_{TP}$ is the two-phase turbulent velocity. It is related to its single-phase counterpart by a "two-phase multiplier" θ :

$$\left(\frac{\varepsilon}{l_m}\right)_{TP} = \theta \left(\frac{\varepsilon}{l_m}\right)_{SP} \tag{8}$$

The multiplier is a function of quality, accounting for the fact that the strength of turbulence depends on the flow regime. It was originally introduced by Lahey[7] who used it in the description of both turbulent mixing and void drift. Since FIDAS uses not Lahey's but Prandtl's mixing theory, the multiplier becomes a measure of the strength of void drift.

Wallis[9] found that inter-channel transfer rates reach a maximum at the slug-annular flow transition; he expressed the transition quality X_m as :

$$X_m = \frac{[\ 0.4 \sqrt{\rho_l(\rho_l - \rho_g) g D_h}\ ]/G + 0.6}{\sqrt{\rho_l/\rho_g} + 0.6} \tag{9}$$

According to Beus[10], the value of θ increases linearly between X=0 and X=X_m and decreases hyperbolically beyond that. At the transition, it reaches the maximum value θ_m, which must be determined empirically. The function, sketched in Fig.5 as the "original model", is formulated as follows :

$$\theta = \begin{cases} 1 + (\theta_m - 1)\ X/X_m & X \leqq X_m \quad (10a) \\ 1 + (\theta_m - 1)\ \left(\dfrac{1 - X_o/X_m}{X/X_m - X_o/X_m}\right) & X > X_m \quad (10b) \end{cases}$$

where $X_o/X_m = 0.57\ Re^{0.0417}$ (11)

The single phase $(\varepsilon/l_m)_{SP}$ is defined by the eddy diffusivity ε and the mixing length l_m in turbulent mixing theory. In the void drift model, however, FIDAS uses a correlation for $(\varepsilon/l_m)_{SP}$ based on the work by Rogers and Rosehart[11] :

$$\left(\frac{\varepsilon}{l_m}\right)_{SP} = -\ \lambda\ Re^{-0.1} \left[1 + \left(\frac{D_{h,j}}{D_{h,1}}\right)^{1.5}\right] \frac{D_{h,1}}{D_r} \frac{G_1}{\sigma} \tag{12}$$

where $\lambda = 0.0058 \left(\frac{S_L}{D_r}\right)^{-1.46}$ (13)

and the Reynolds number Re and the density are based on the two-phase mixture.

4.2 Determination of Suitable Mixing Length and Void Drift Parameters

An attempt was made to find suitable values of K_1 for the mixing length and K_2, X_m, θ_m for the void drift in advance of the validation study.

The turbulent mixing rate in single-phase flow obtained in various subchannel configuration by several researchers were summarized by Hori et al.[12]. This result was used to decide a suitable value for the mixing length in single-phase flow. In Fig.3, the experimental data indicate the mixing parameter (ε / ν) is insensitive to subchannel configuration and gap width within the experimental range. Therefore, analysis was made for the experiment of Hori et al.(for case =1=) with gap width of 2.0mm. As shown in the figure, predictions by FIDAS with different mixing length are compared with measured mixing coefficient. The most suitable mixing length appears to be one quarter of hydraulic diameter, i.e. $K_1 = 1/4$.

In addition to the single-phase experiments, flow distributions in an air/water two-phase flow were measured in order to demonstrate the void drift phenomenon by Sato and Sadatomi[13] in adjacent subchannels of different cross-section. These results are shown in Fig.4, along with measurements by other researchers on similar subchannel pairs.(see ref.[13]) In general, the strength of void drift is known to be dependent on flow regime. As shown in Fig.4, large separation of gas and liquid occurred in the slug flow region (due to void drift), but there was little separation with bubbly or annular flow. The experimental data reveal that the separation effect is independent of subchannel configuration.

In predicting this trend with the FIDAS code, the value of

X_m, θ_m and K_2 in the correlation were systematically changed until the best fit was obtained. The most suitable values of mixing length in bubbly and slug flow appear to be 1.5 times the hydraulic diameter for liquid film and to be 1/100 of the hydraulic diameter (i.e. K_1=1/100) for the gas phase which is discontinuous. As expected, the mixing length for the liquid phase in bubbly and slug flow is larger than that for single-phase liquid flow, presumably due to enhanced mixing by bubbles. The suitable value of X_m was also found to be 1/4 that of the transition quality recommended by Wallis and defined in equation (9). This suggests that the maximum void drift occurs in the slug flow region, not at the slug-annular transition. In addition, a suitable value of θ_m could be obtained by the following equation as a function of the superficial liquid velocity.

$$\theta_m = 37(j_1/j_{1,o} - 1.0)^2 + 13 , \qquad (14)$$

where $j_{1,o}$ is 1.0m/s.

Figure 5 compares the original correlation by Beus with the variations that were examined. It is hypothesized that the original trend is correct, but that different θ_m and X_m values are more suitable. Also, the recommended value of K_2 is 1.4.

Comparisons between prediction by FIDAS and measurements are also indicated in Fig.4. The predicted values by FIDAS trace well the measured trend of flow distributions in two-phase flow which are the result of diversion cross flow, turbulent mixing and void drift.

5. EXPERIMENTAL DATA AND CALCULATIONAL PROCEDURE

Two sets of experiments were used for comparison with code predictions : the General Electric (GE) 9-rod bundle measurements by Lahey et al.[7], and the ISPRA 16-rod bundle measurements by Herkenrath and Hufschmidt[8]. In both sets, flow quality and mass flux were measured in various subchannels of a square-

lattice bundle, in which electrically heated rods simulated nuclear fuel rods. Measurements were made using flow splitters and an isokinetic probe technique. The flow conditions were that of a normally operating boiling water reactor, in which the coolant reaches bubbly and slug flow. The main differences between the GE and ISPRA tests were the bundle size (9 and 16 rods respectively) and the bundle length (1.80 and 3.66 m). The cross-sections for the test bundles are shown in Fig.6.

In the General Electric experiments, tests were also performed with a non-uniform cross-bundle heating distribution. This was considered to be more representative of the non-uniform power profile in an actual reactor core. However, these data were not used in present study, since non-uniform tests are considered to be less reliable than uniformly heated tests.

Table 3 compares the subchannel dimensions of the GE and ISPRA rod bundles; similar D_h/D_r diameter ratios indicate that similar flow distributions can be expected in the two experiments. The conditions of pressure, mass flux, power, and inlet enthalpy under which the tests were performed are listed in Table 4.

Before discussing the results of the validation, it is instructive to review the important trends of the experiment. The experiment indicates that the mass flux in the corner subchannel is lower than the bundle average for both single- and two-phase flow. Moreover, the most significant phenomenon observed in the experiment is that the quality in the corner subchannel is much lower than the bundle average. This occurs in spite of the fact that the power-to-flow ratio is highest for the corner subchannel. This is due to the presence of an unheated liquid film on the outer wall, and due to the tendency of its bubbles to move out to high velocity vapor streams in the larger channels. Mass flux through the corner is lower than average for the same reasons. Conversely, center subchannels - due to size and location - are characterized by higher than average quality and mass flux.

The error in mass balance (between average bundle mass flux and total subchannel mass flux) was found to be less than 5 % for

the GE measurements with uniform heat. Such continuity could not be checked for the ISPRA data, because not all representative subchannels were tested.

The subchannel configurations used in the present analysis are indicated in Fig.6 for both of GE and ISPRA tests. The conventional coolant-centered subchannel layout is used in present study for comparison with other codes described later, although one can use not only coolant-centered but also rod-centered or combined-fine subchannel layouts in FIDAS. The axial and lateral mesh structures used are presented in Fig.7. The number of physical cells (axial nodes) is 40, and as a result, axial node length is approximately 50mm which had been confirmed to be short enough according to parametric studies done in advance of validation analysis to examine the numerical error. The length of the lateral junction is defined as the distance between mass centers of adjacent subchannels.

6. RESULTS ON THE CODE AND MODEL ASSESSMENT

6.1 GE 3x3 Rod Bundle Test Analysis

The comparisons of predictions by FIDAS with the measurements in GE 3x3 rod bundle test are found in Figs.8, 9, 10 and 11. It is seen in Fig.8 that the single-phase mass flux in the corner subchannel is satisfactorily predicted in the case of $K_1=1/4$ in Eq.(5) for the value of the mixing length $l_m= D_h/4$. Comparisons of two-phase mass flux prediction by FIDAS with the measurements are also indicated in Fig.9. The predicted mass fluxes for the corner, center and side subchannels are in fairly good agreement with the data. Additionally, comparisons of quality distribution as a function of the bundle average quality are illustrated in Fig.10. The predicted values follow the trend of the data satisfactorily. Finally, the comparisons are summarized for all measurement in GE 3x3 uniformly heated test in Fig.11.

6.2 ISPRA 4x4 Rod Bundle Test Analysis

The comparisons of predictions by FIDAS with the measurements in ISPRA 4x4 rod bundle test are found in Figs.12, 13 and 14. It is shown in Figs.12 and 13 that predictions by FIDAS trace the data trend of the corner and side-center subchannels qualities satisfactorily. In particular, the predicted values coincide with the dependence of corner subchannel quality on bundle average mass flux. In Fig.14, the comparisons are also summarized for ISPRA 4x4 test.

Hence, through the above mentioned validation, the present mixing model in FIDAS is recognized to be appropriate.

7. DISCUSSION

Quality and mass flux measurements with the 9-rod [7] and 16-rod [8] bundles have been widely used for the validation of thermalhydraulic subchannel codes. Two of these, THERMIT-II and COBRA-IV, are compared here with FIDAS in the prediction of quality and mass flux under normal reactor operating conditions. The two-phase models of the codes are compared in Table 5.

COBRA-IV[14] assumes a homogeneous vapor/liquid mixture. Turbulent mixing between subchannels is described by a "mixing parameter"; for the COBRA results shown in this section, the parameter has been fine-tuned to suit rod bundles. COBRA does not model the separation of phases due to void drift phenomenon.

THERMIT-II[1] is similar to FIDAS, but it is a two-fluid code which uses empirical correlations for dryout, and does not simulate entrained droplets as a third fluid. The code relies on Lahey's turbulent mixing model (instead of Prandtl's) with Beus' correlation for the two-phase mixing multiplier, but it uses the same void drift model as FIDAS. Both turbulent mixing and void drift models have been fine-tuned in THERMIT by comparisons with the GE and ISPRA tests.

Predictions of subchannel qualities and mass fluxes by each code are compared with measured data in Figs. 12 to 13 for the ISPRA and in Figs.15 to 17 for the GE tests.

It is generally believed that quality and mass flux for the

corner subchannel are the most difficult to predict accurately. Since the corner has the smallest size and the highest power density, it is most sensitive to flow conditions. According to the previous set of figures, quality and mass flux in the side, center, or side-center subchannels of the uniformly heated bundles are generally well predicted by each code. Figures 13 and 15 indicate this trend. However, discrepancies of code predictions appear with the corner subchannel conditions.

As shown in Figs. 12 and 16, FIDAS traces well the experimental data of corner subchannel quality. THERMIT also succeeds reasonably well in the prediction, but FIDAS provides a better fit. COBRA fails to represent the quality accurately. This is due to the absence of void drift modeling, in which case turbulent mixing dominates completely and the subchannel quality approaches average bundle quality. However, for the corner mass flux shown in Fig.17, each code is able to predict within the bounds of experimental uncertainty.

In general, FIDAS gives better predictions in comparison with other codes for subchannel quality and mass flux under normal reactor operating conditions. It is considered that this improvement depends on the three-fluid modeling in which suitable values of mixing length for each phases and void drift parameters can be defined. Indeed, the fact that FIDAS considers droplets as a third fluid and offers mechanistic (rather than empirical) dryout and heat transfer models may make it a better code for simulations of dryout and post-dryout heat transfer in rod bundles.

8. CONCLUSIONS

Validation of the two-phase mixing models consist of turbulent mixing, diversion cross flow and void drift in FIDAS-3DT has been performed. In the turbulent mixing model, the most suitable mixing length values were found for single-phase liquid and each phase in two-phase flow. With the void drift model including the two-phase multiplier obtained in present study which describes dependence on the flow-regime, measured

subchannel flow distribution due to void drift phenomenon were well traced.

Comparisons with 9-rod and 16-rod fuel bundle experiments have shown that the FIDAS code is generally successful in predicting quality and mass flux in subchannels. The predictions also show better accuracy when compared with those by the THERMIT-II and COBRA-IV subchannel codes.

Consequently, the FIDAS-3DT code appears to be suitable for simulating quality and mass flux distribution in rod bundles.

ACKNOWLEDGMENT

The authors would like to express their appreciation to Dr. K.Shiba for his support of this research effort. The author thanks Mr. H.Kato, Mr. K.Fukugami for their vigorous assistance in the analytical calculations.

NOMENCLATURE

$\overline{A}$	=	interfacial area per unit volume (1/m)
D	=	diameter (m)
F	=	lateral momentum flux (kg/m s^2)
f	=	friction factor (-)
g	=	gravitational acceleration (=9.81 m/s^2)
G	=	axial mass flux (kg/m^2 s)
h	=	specific enthalpy (kJ/kg)
j	=	superficial velocity (m/s)
K_1	=	mixing length constant (-)
K_2	=	void drift constant (-)
L	=	lateral length (m)
l_m	=	mixing length (m)
m_B	=	suppression rate of droplets deposition by evaporation (kg/m^2·s)
m_D	=	deposition rate of droplets onto the liquid film (kg/m^2·s)
m_E	=	entrainment rate of droplets from the liquid film by roll waves (kg/m^2·s)
P	=	pressure (Pa, MPa)
Pr	=	Prandtl number (-)
$\dddot{Q}$	=	heat transferred per unit volume (W/m^3)
q	=	heat flux (W/m^2)
$\dddot{q}_I$	=	interfacial heat flux per unit volume (W/m^3)
q_L	=	lateral energy mixing rate (kJ/m s)
Q_L	=	lateral energy flux (kJ/m^2 s)
Re	=	Reynolds number (-)
S	=	entrainment rate per unit volume (kg/m^3·s)
Sc	=	Schmidt number (-)
S_L	=	gap length between rods (m)
t	=	time (s)
t_F	=	film thickness (m)
u	=	axial velocity (m/s)
v	=	lateral velocity (m/s)
We	=	Weber number (-)
w	=	lateral mass mixing rate (kg/m s)

X = steam quality (-)
z = axial length (m)

Greek letters

α = volume fraction (-)
Γ = evaporated or condensed mass ($kg/m^3 \cdot s$)
η = evaporation coefficient (-)
ε = diffusion coefficient (m^2/s)
μ = dynamic viscosity (NS/m^2)
ν = kinematic viscosity (m^2/s)
ρ = density (kg/m^3)
σ = surface tension (N/m)
τ = shear stress (N/m^2)
$\dddot{\tau}$ = shear force per unit volume (N/m^3)
τ_L = lateral shearing rate (kg/s^2)
θ = two-phase multiplier for void drift (-)

Sub/Superscripts

E = entrainment or energy
F = liquid film
G = gas core
g = gas phase
h = hydraulic
i = subchannel i
j = subchannel j
k = phase
l = liquid phase
L = lateral
m = mixing or maximum
M = mass
r = rod
SP = single-phase
T = turbulent
TP = two-phase
U = momentum

X = axial

W = wall

REFERENCES

[1] Ishii, M., Thermo-fluid dynamic theory of two-phase flow, Eyrolles, Paris(1975).

[2] Kelly, J.E., Kao, S.P. and Kazimi, M.S., THERMIT-2: A two-fluid model for light water reactor subchannel transient analysis, MIT-EL-81-014(1981).

[3] Thurgood, M.J., Kelly, J.M., Guidotti, T.E., Kohrt, R.J. and Crowell, K.R., COBRA/TRAC - A thermal-hydraulics code for transient analysis of nuclear reactor vessels and primary coolant systems, NUREG/CR-3046(1983).

[4] Sugawara, S., Droplet deposition and entrainment modeling based on the three-fluid model, the 3rd Int. Nat. Top. Mtg. on Nuclear Reactor Power Plant Thermal Hydraulics and Operations, Seoul, Korea, p.A1-19 to p.A1-28(1988).

[5] Sugawara, S. and Miyamoto, Y., FIDAS: Detailed subchannel analysis code based on the three-fluid and three-field model, submitted to the Journal of Nuclear Engineering and Design (special issue for Recent Japanese Advances in the Area of Nuclear Reactor Thermal-Hydraulics and Related Safety), October(1988).

[6] Tso, C.P. and Sugawara, S., An analysis of annular two-phase three-field horizontal flow, the 3rd Int. Symp. on Transport Phenomena in THERMAL CONTROL, Taipei, pp.369-376(1988).

[7] Lahey, R.T. Jr., Shiralkar, B.S. and Radcliffe, D.W., Mass flux and enthalpy distribution in a rod bundle for single- and two-phase flow conditions, J. of Heat Transfer(May, 1971), 197-209.

[8] Herkenrath, H., Hufschmidt,W., Jung, U. and Weckermann, F., Experimental investigation of the enthalpy and mass flux distribution in 16-rod clusters with BWR and PWR geometries and conditions, EUR 7575EN (1981).

[9] Wallis, G.B., One-dimensional two-phase flow, McGraw-Hill(1969).

[10] Beus, S.G., Two-Phase Turbulent Mixing Model for Flow in Rod Bundles, WAPD-T-2438 (1970).

[11] Rogers, J.T. and Rosehart, R.G., Mixing by Turbulent Interchange in Fuel Bundles - Correlations and Inferences, ASME, 72-HT-53 (1972).

[12] Hori, K., Kato, S. and Kitahara, T., A study on a single-phase turbulent mixing in subchannels which have equal flow areas, Proceedings of Japan Heat Transfer Symp., pp.105-108(1982).

[13] Sato, Y., Sadatomi, M. and Tsukashima, H., Two-phase flow characteristics in interconnected subchannels with different cross-sectional areas", 2nd Int. Topical Meeting on Nuclear Power Plant Thermal Hydraulics and Operation, Tokyo, April 1986.

[14] Stewart, C.W., Wheeler, C.L. et al., COBRA-IV : The Model and the Method, Battelle Pacific Northwest Laboratories, Report No. BNWL-2214 (1977).

[15] Lahey, R.T. Jr. and Moody, F.J., The thermal-hydraulics of a boiling water nuclear reactor, ANS(1977).

Table 1 Field Equations

Conservation of Mass (3 equations)

$$\frac{\partial}{\partial t}(\alpha_k\rho_k) = -\nabla(\alpha_k\rho_k u_k) + \Gamma + S \ , \tag{1-1}$$

and, $$\sum_k \alpha_k = 1 \ . \tag{1-2}$$

Conservation of Energy (3 equations)

$$\frac{\partial}{\partial t}(\alpha_k\rho_k h_K) = -\nabla(\alpha_k\rho_k h_k u_k) - \nabla[\alpha_k(q_k + q_k^T)]$$

$$+ \Gamma\, h_k + \dddot{q}_{Ik} + \dddot{Q}_{Wk} + \alpha_k \frac{\partial P}{\partial t} \ . \tag{1-3}$$

Conservation of Momentum (6 equations)

(Axial Momentum)

$$\frac{\partial}{\partial t}(\alpha_k\rho_k u_k) = -\nabla_x(\alpha_k\rho_k u_k u_k) - \frac{1}{A}\sum_n(\alpha_k\rho_k u_k v_k S_L)_n$$

$$- \alpha_k\nabla_x P - \alpha_k\rho_k g_k + (\dddot{\tau}_I)_x + (\Gamma u)_x$$

$$- \nabla_x(\alpha_k\tau_{kxx}) + \frac{1}{A}\sum_n(\alpha_k\tau_{kLx}S_L)_n \ . \tag{1-4}$$

(Lateral Momentum)

$$\frac{\partial}{\partial t}(\alpha_k\rho_k v_k) = -\nabla_L(\alpha_k\rho_k v_k v_k) - \nabla_x(\alpha_k\rho_k v_k u_k)$$

$$- \nabla_s(\alpha_k\rho_k v_k v_k') - \alpha_k\nabla_L P - \alpha_k\rho_k g_L$$

$$+ (\dddot{\tau}_I)_L + (\Gamma u)_L - \nabla_L(\alpha_k\tau_{kLL}) - \nabla_x(\alpha_k\tau_{kLx}) \ . \tag{1-5}$$

Table 2 Constitutive Equations

Wall-liquid drag force

$$\tau_{WF} = \bar{A}_{WF}\, f_{WF}\, \frac{\rho_F}{2}\, u_F^2 \quad , \text{ in Pa/m}$$

f_{WF} = Blasius' expression

$$= \frac{1}{4}\left(\frac{0.316}{Re_F^{0.25}}\right) \quad , \text{ dimensionless}$$

Vapor-liquid drag force

$$\tau_{FG} = \bar{A}_{FG}\, f_{FG}\, \frac{\rho_G}{2}\, (u_G - u_F)^2$$

f_{FG} = Wallis' expression

$$= \frac{1}{4}\left(\frac{0.316}{Re_G^{0.25}}\right)\left(1 + 300\,\frac{t_F}{D}\right)$$

Vapor-droplet drag force

$$\tau_{EG} = \bar{A}_{EG}\, K_{EG}\, \frac{\rho_G}{2}\, (u_G - u_E)^2$$

$$K_{EG} = \frac{24}{Re_E}\left(1 + 0.15\, Re_E^{0.687}\right) + \frac{0.42}{1+4.25\times10^4 Re_E^{-1.16}}$$

Droplet size

$$D_E = \begin{cases} \dfrac{\sigma\, We}{\rho_G (u_G - u_E)^2} \\ 10^{-3} \quad , \text{ if } D_E < 10^{-3} \end{cases}$$

where We = Weber number (=5)

Table 3 Subchannel Dimensions for GE and ISPRA-BWR Tests

subchannel	flow area (mm^2)	hydraulic diameter D_h (mm)	D_h/D_r (-)
GE corner	49.1	7.0	0.49
ISPRA corner	52.9	7.1	0.47
GE side	119.4	11.6	0.81
ISPRA side	123.6	11.5	0.76
GE center	190.0	16.9	1.18
ISPRA center	203.5	17.3	1.15

bundle	rod diam. D_r (mm)	rod gap (mm)	wall gap (mm)
GE	14.3	4.42	3.51
ISPRA	15.0	4.50	3.37

Table 4 Experimental Conditions for GE and ISPRA-BWR Tests

	GE 9-rod bundle (non-uniform heating)	GE 9-rod bundle (uniform heating)	ISPRA 16-rod bundle (uniform heating)
Pressure (MPa)	7.0	7.0	7.0
Mass Flux (kg/m^2s)	725 1450	725 1450	1000 1500 2000
Bundle Power (kW)	530 - 1060 radially non-uniform	530 - 1600	320 - 1600
Subcooling (kJ/kg)	210 - 640	70 - 600	40 - 110
Average Exit Quality (%)	3.2 - 10.0	2.9 - 31.8	2.0 - 31.0

Table 5 Comparison of Two-Phase Flow Model between Codes

code	2-phase flow model	mixing model			dryout prediction
		turb. mix	cross flow	void drift	
FIDAS-3DT	3-fluid	○	○	○	mechanistic
COBRA-IV	1-fluid (HEM)	○	○	×	empirical
THERMIT-II	2-fluid	○	○	○	empirical

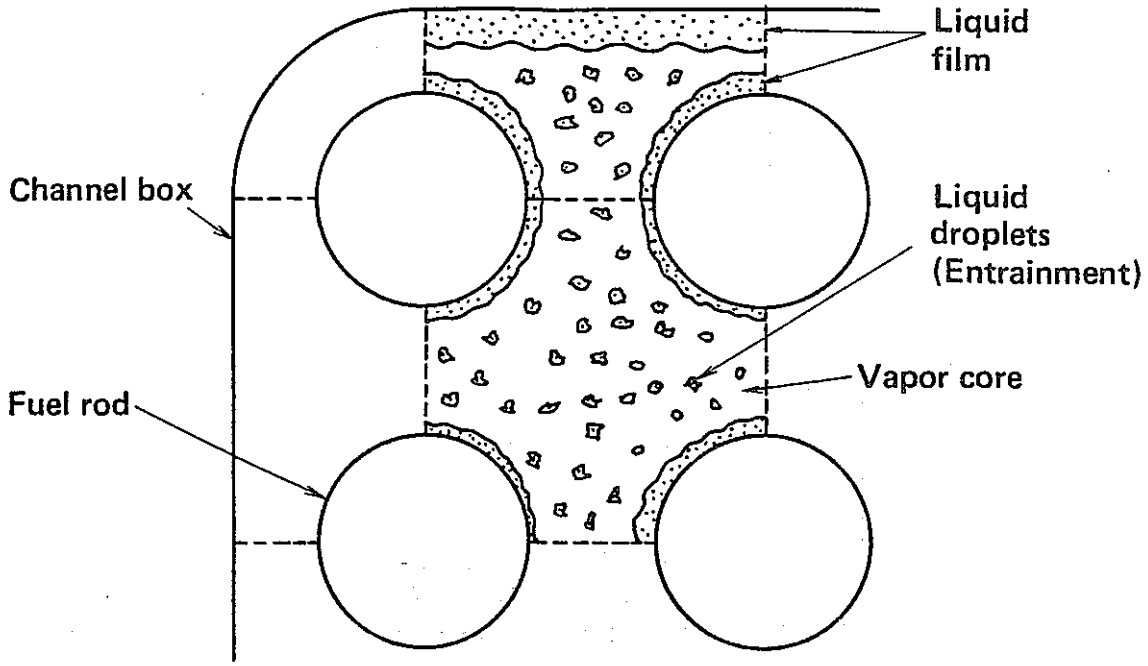

(a) Three-fluid Model for Rod Bundle

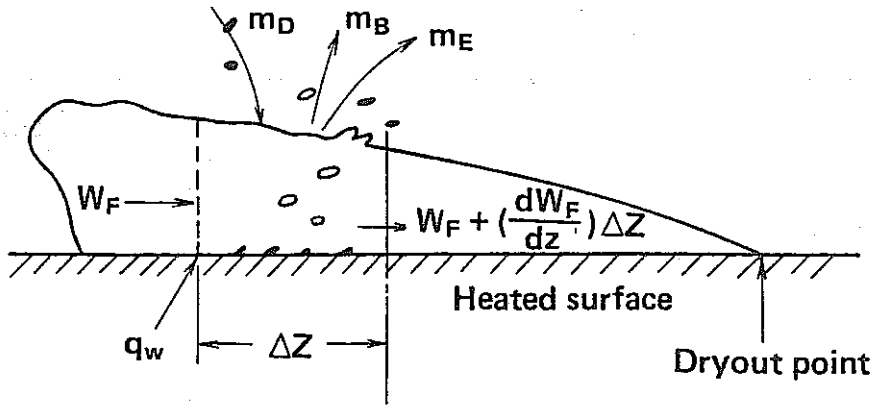

(b) Film Dryout Model

Fig. 1 Three-Fluid and Film Dryout Modeling in FIDAS

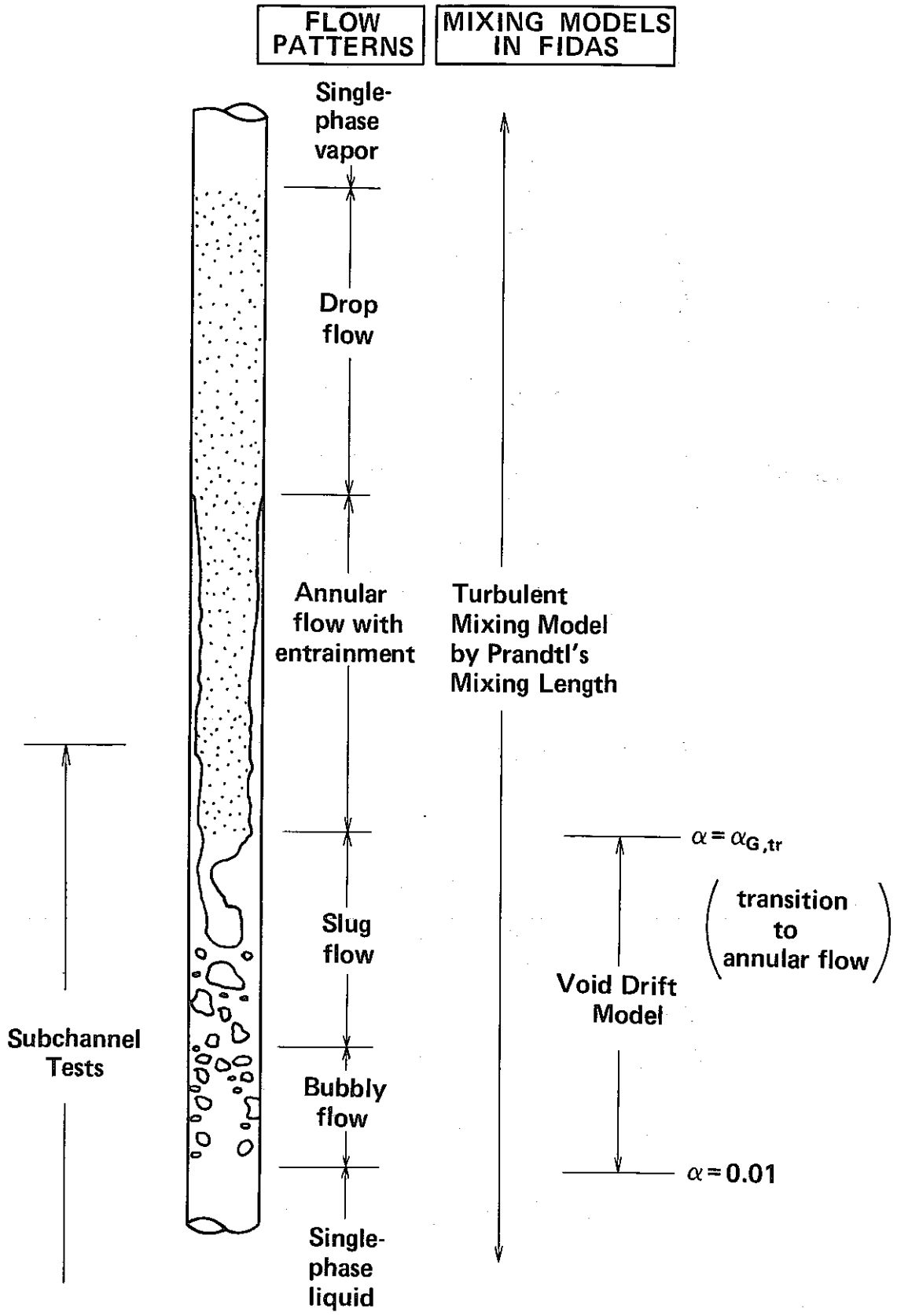

Fig. 2 Two-Phase Flow Regimes in A Heated Channel

	=1=	=2=	=3=	=4=	=5=	=6=
Researcher	Hori et al.	Sekoguchi et al.	Sekoguchi et al.	Hetsroni et al.	Petrunik	Hori et al.
Geometry	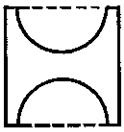	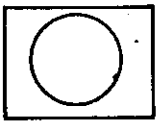	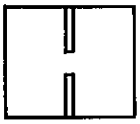	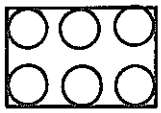	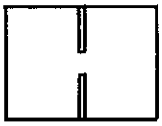	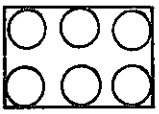
Gap (mm)	1.5 2.0 3.0	1.0 2.0	1.85	2.5	2.54	2.5
D_h (mm)	6.48 6.83 7.53	9.72 11.5	14.5	5.09	19.81	9.84

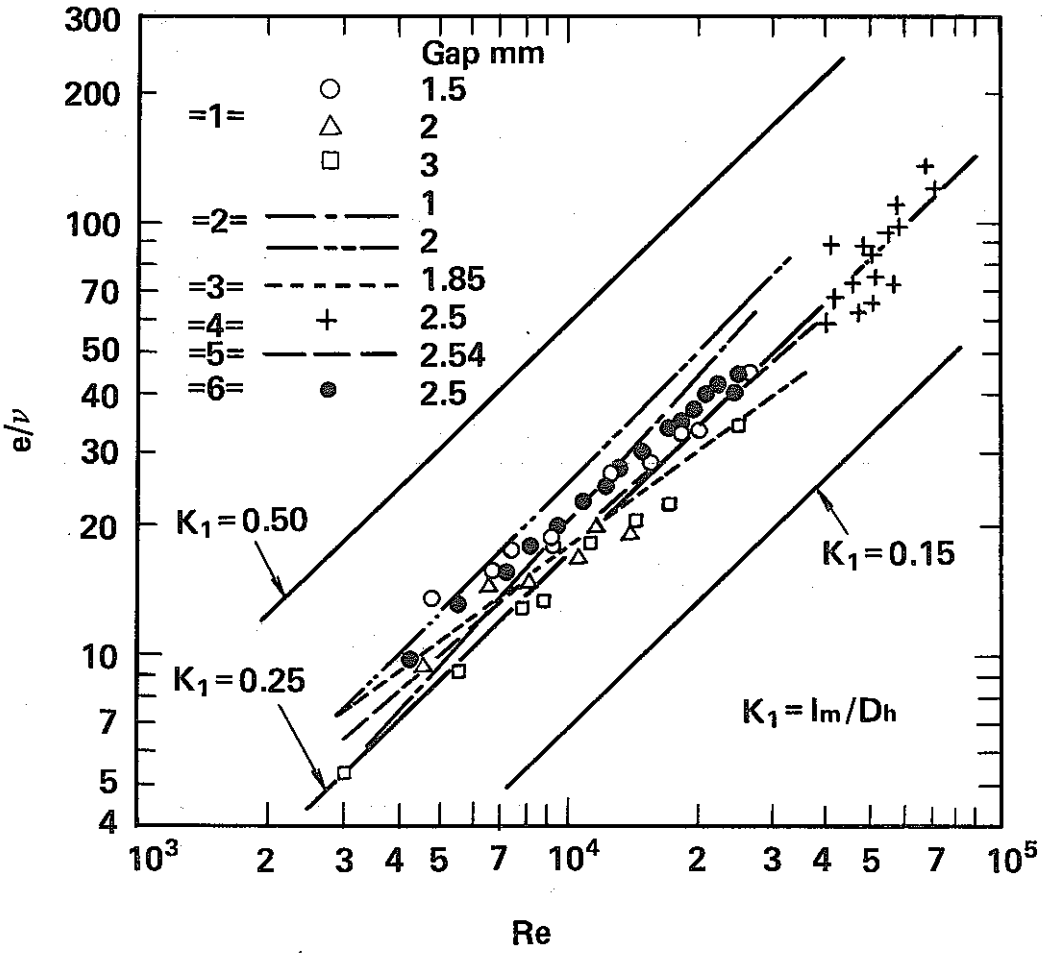

Fig. 3 Mixing Length and Turbulent Mixing Rate in Single-Phase Flow [12]

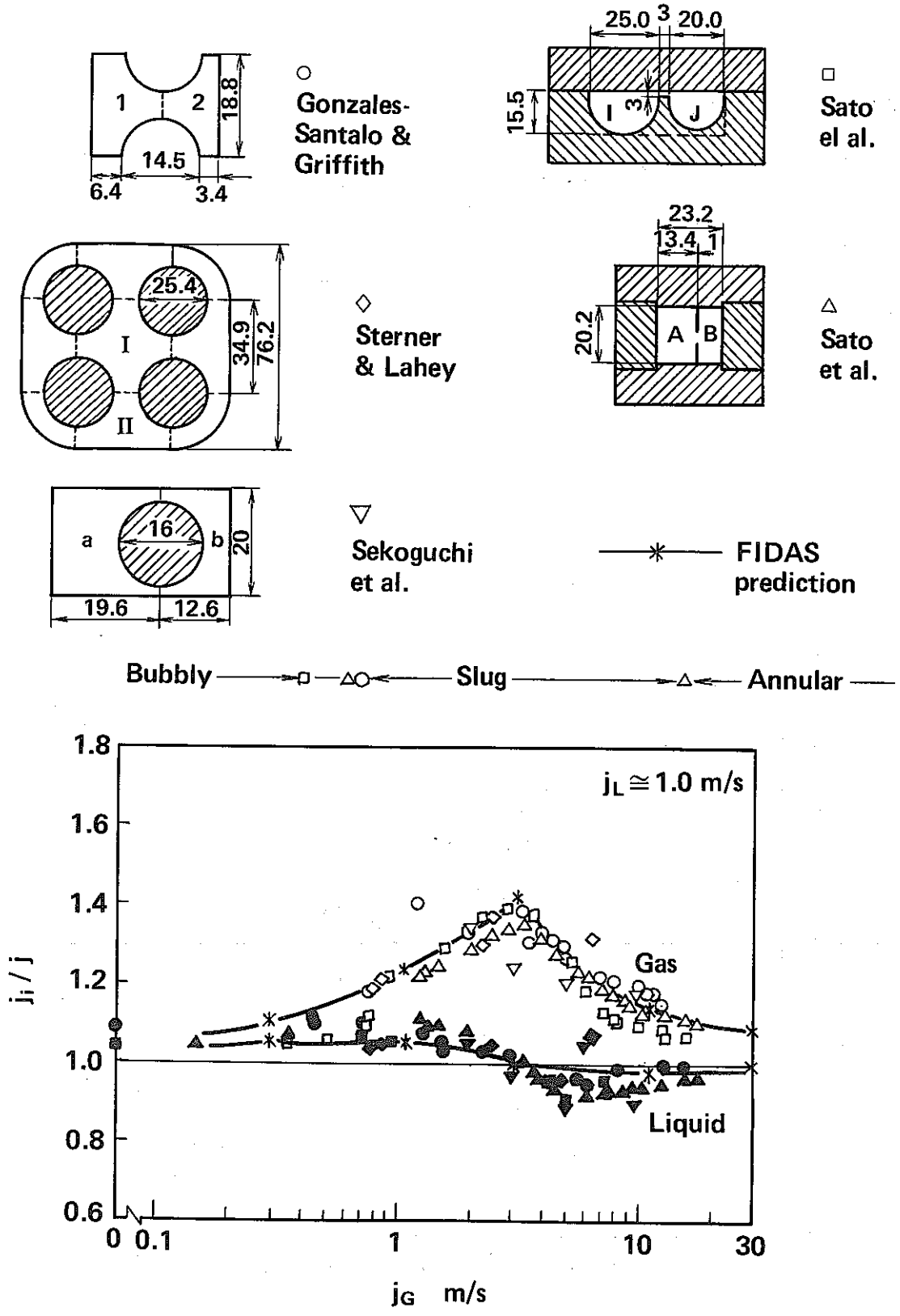

Fig. 4 Flow Distributions in the Larger Subchannel of Various Subchannel Pairs [13]

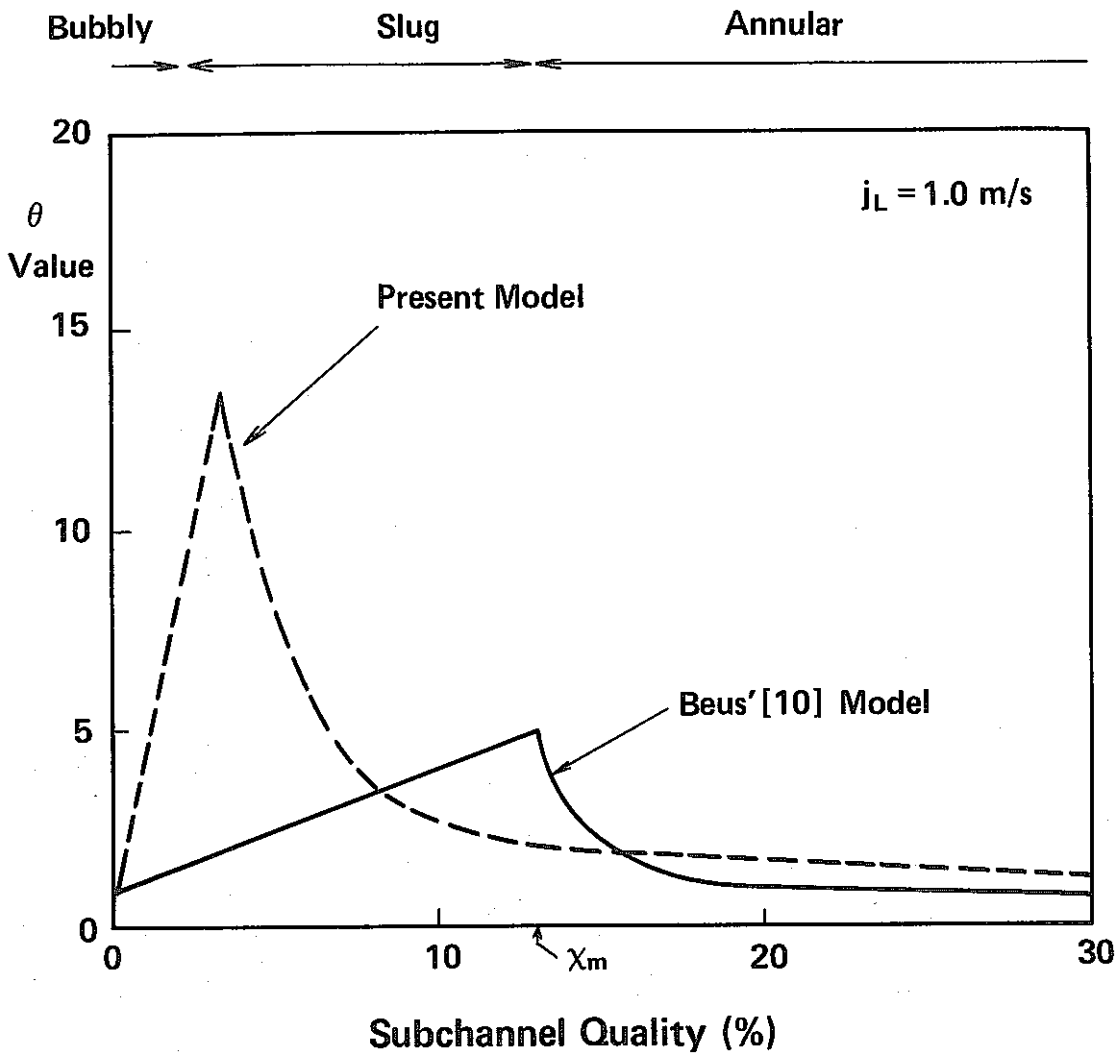

Correlation	θ_m	χ_m
Original	5	χ_m
Present Model	13	$0.22\,\chi_m$

Fig. 5 Variations of θ_m, χ_m for θ Correlation

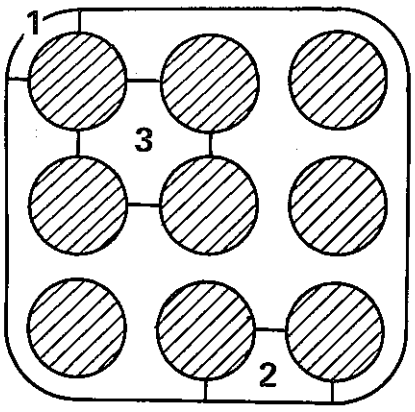

GE 9-rod bundle

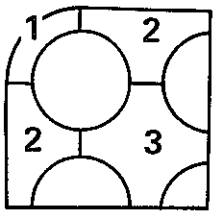

1 Corner
2 Side
3 Center

Configuration for
Code Analysis

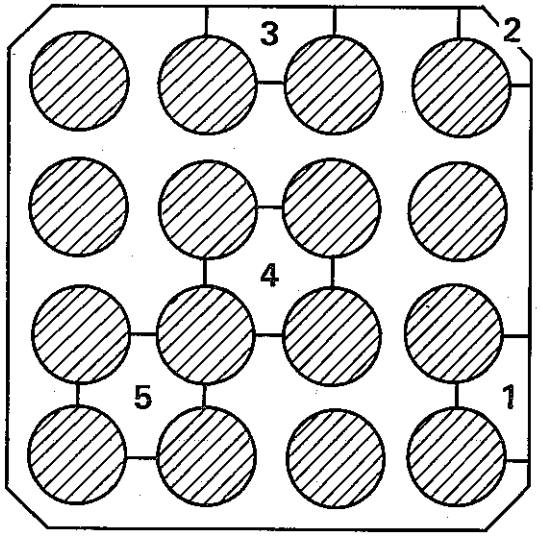

ISPRA 16-rod bundle

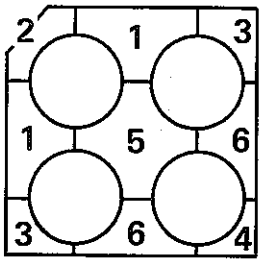

1 Side
2 Corner
3 Side
4 Center
5 Side-Center

Configuration for
Code Analysis

Fig. 6 Test Sections for GE 3×3 and ISPRA 4×4 Rod Bundles

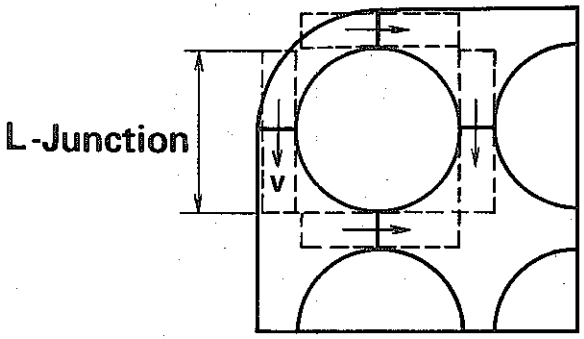

Sectional Mesh

Position	Parameter
X-Node	α_G , α_E , α_F h_G , h_E , h_F P
L-Junction	u_G , u_E , u_F
X-Junction	v_G , v_E , v_F

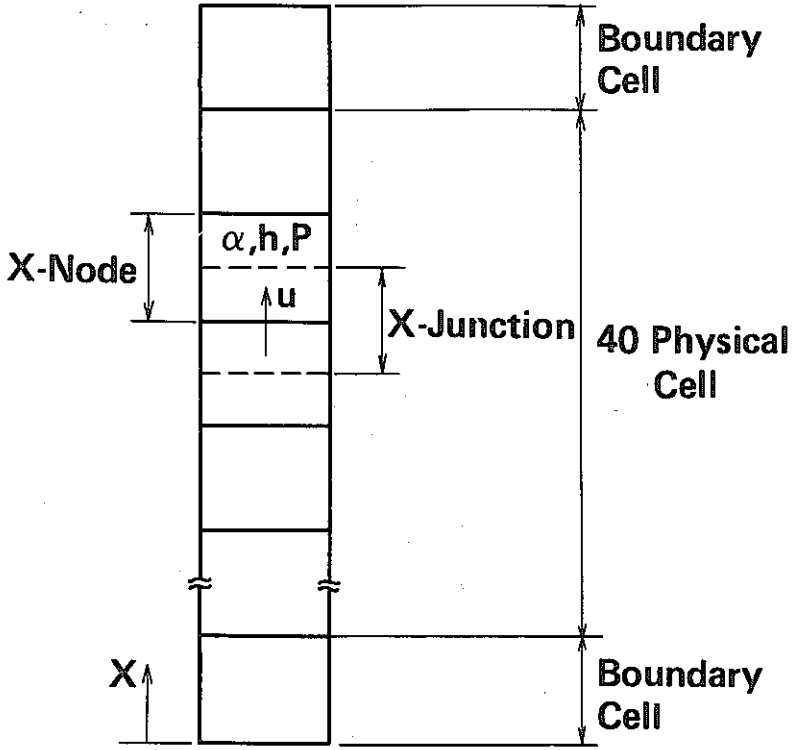

Axial Mesh

Fig. 7 Mesh Structure for Test Section

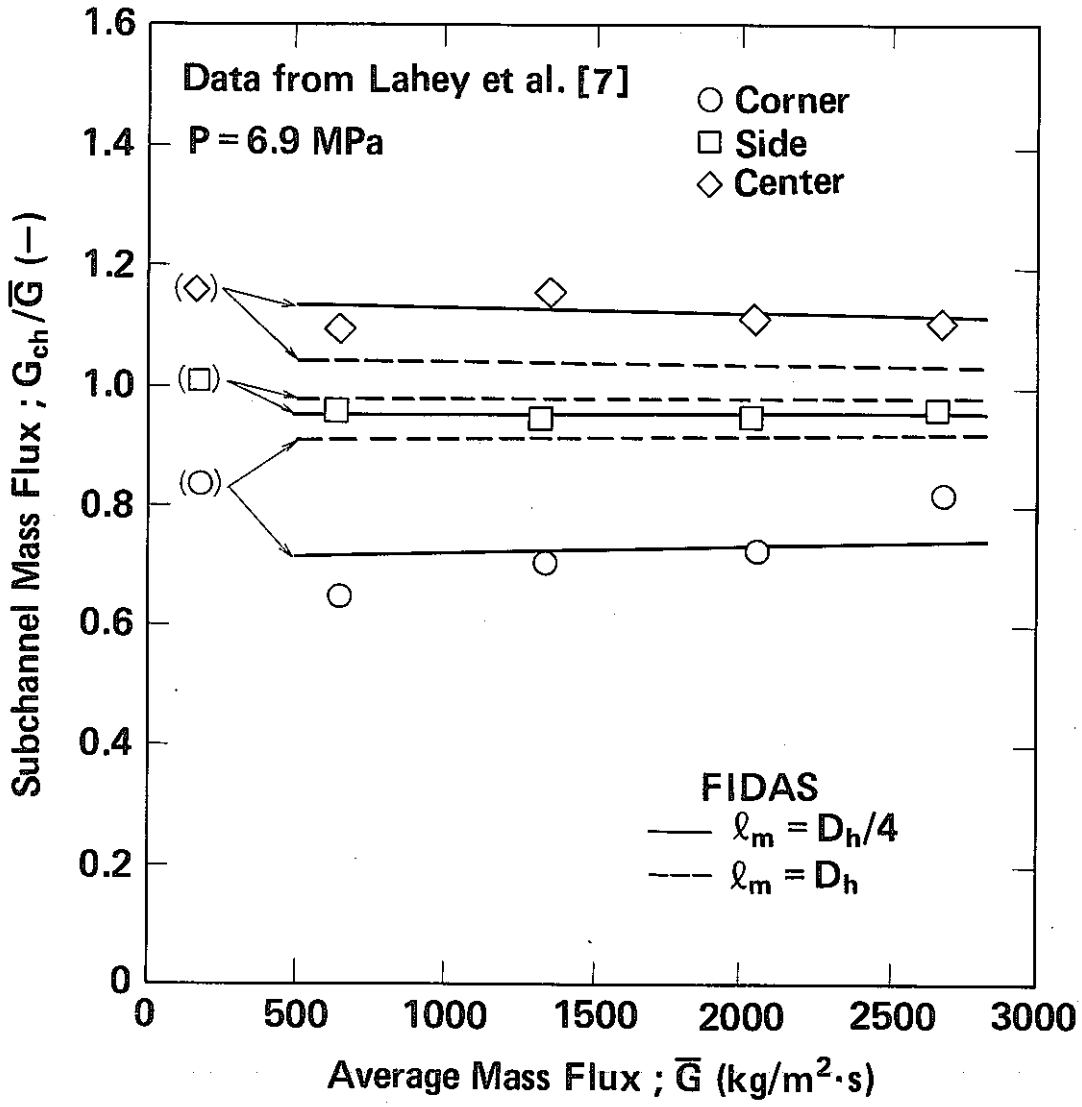

Fig. 8 Predicted and Measured Subchannel Mass Flux Distribution in Single-Phase Flow for GE 3×3 Rod Bundle Test

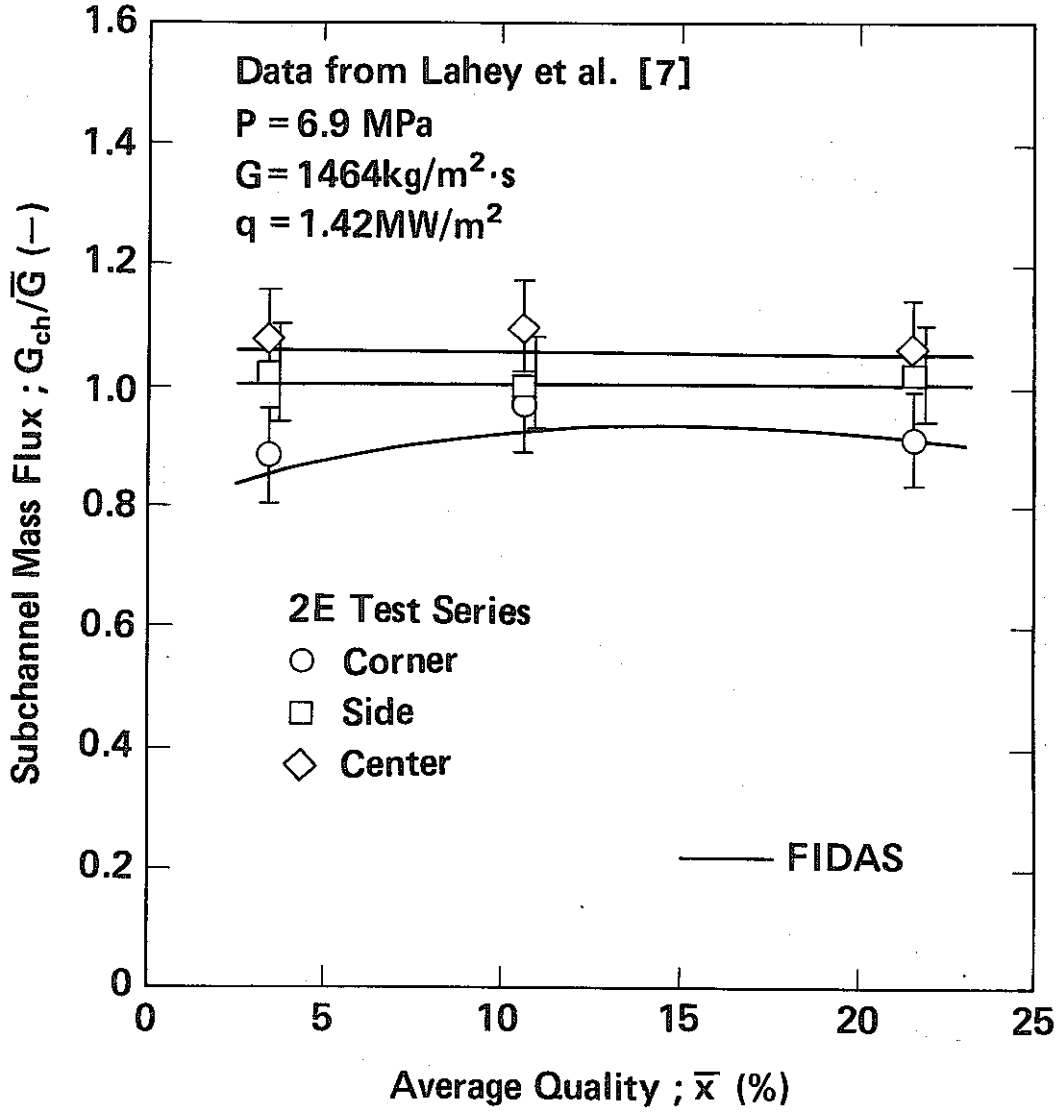

Fig. 9 Predicted and Measured Subchannel Mass Flux Distribution in Two-Phase Flow for GE 3×3 Rod Bundle Test

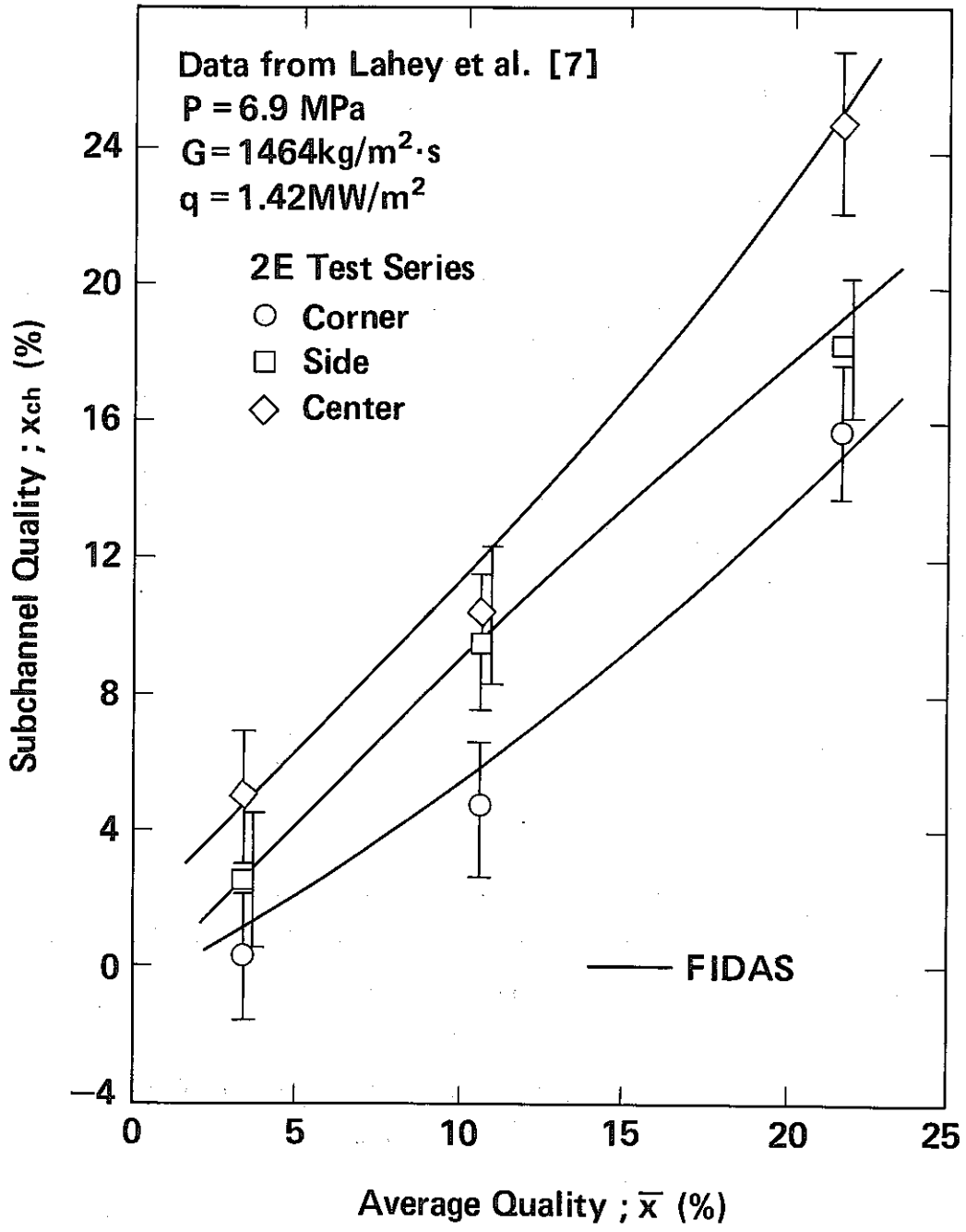

Fig. 10 Predicted and Measured Subchannel Quality Distribution in Two-Phase Flow for GE 3×3 Rod Bundle Test

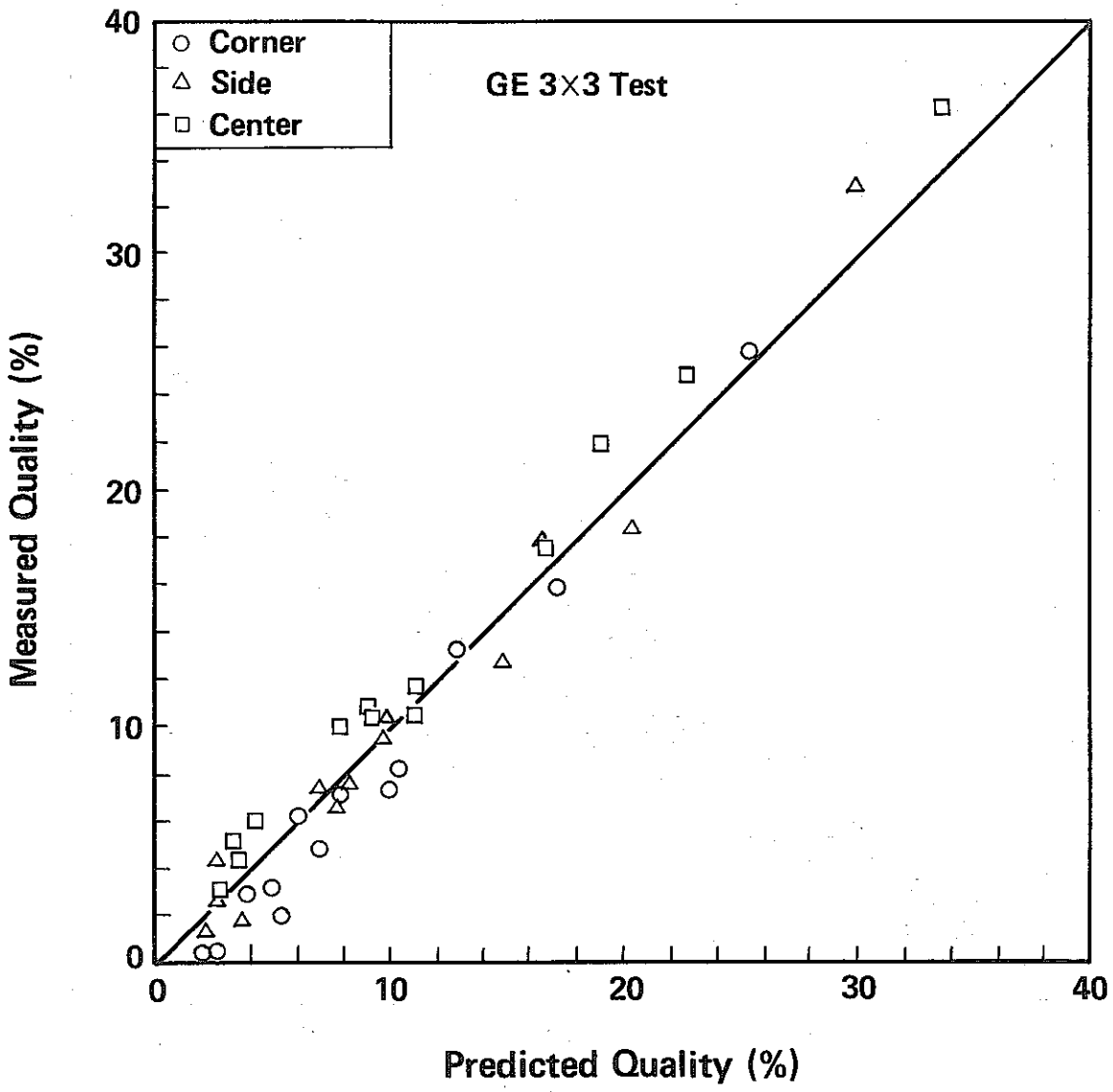

Fig. 11 Predicted and Measured Qualities for GE uniformly Heated Subchannels

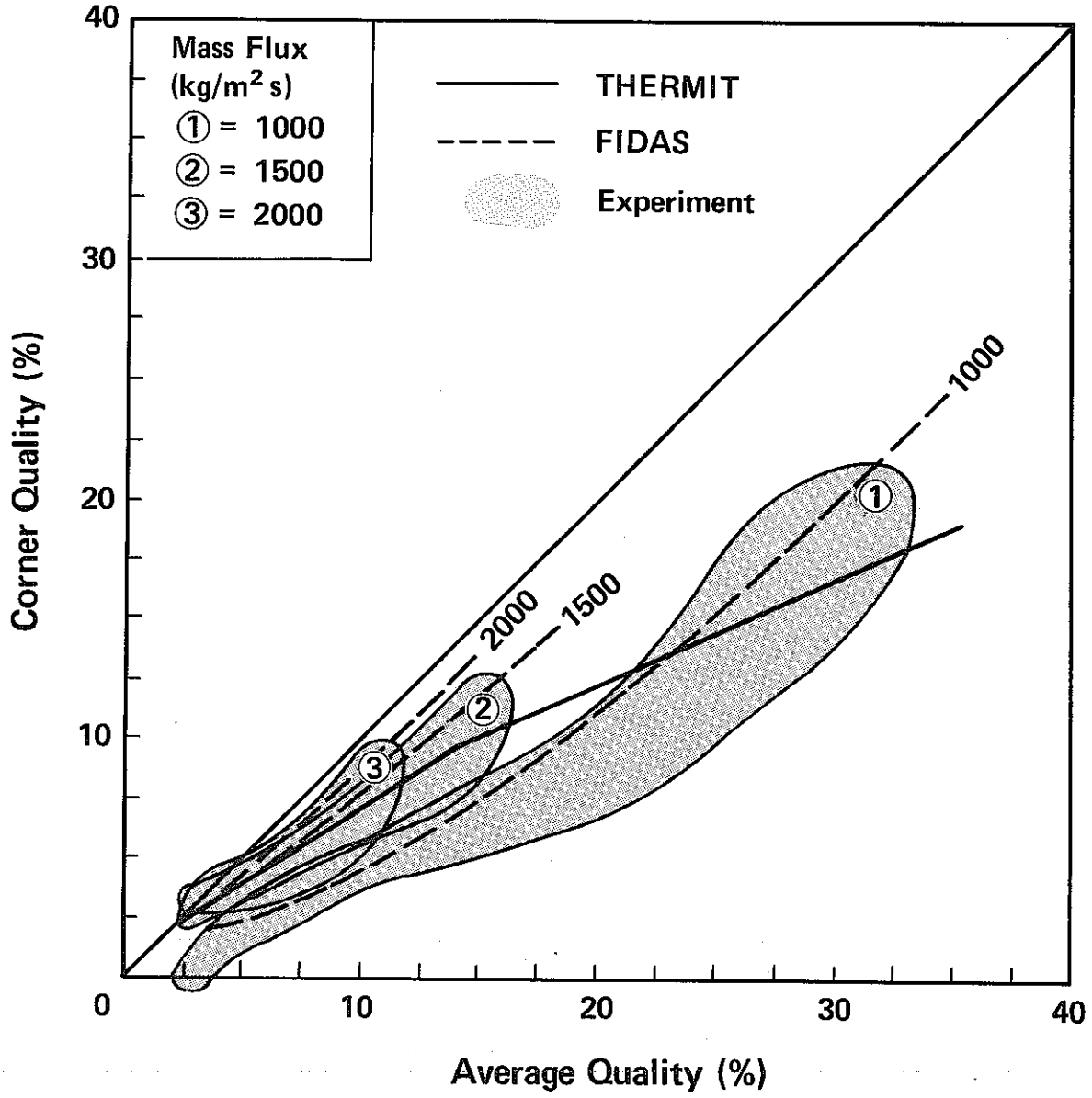

Fig. 12 Predicted and Measured Qualities for ISPRA-BWR Corner Subchannels

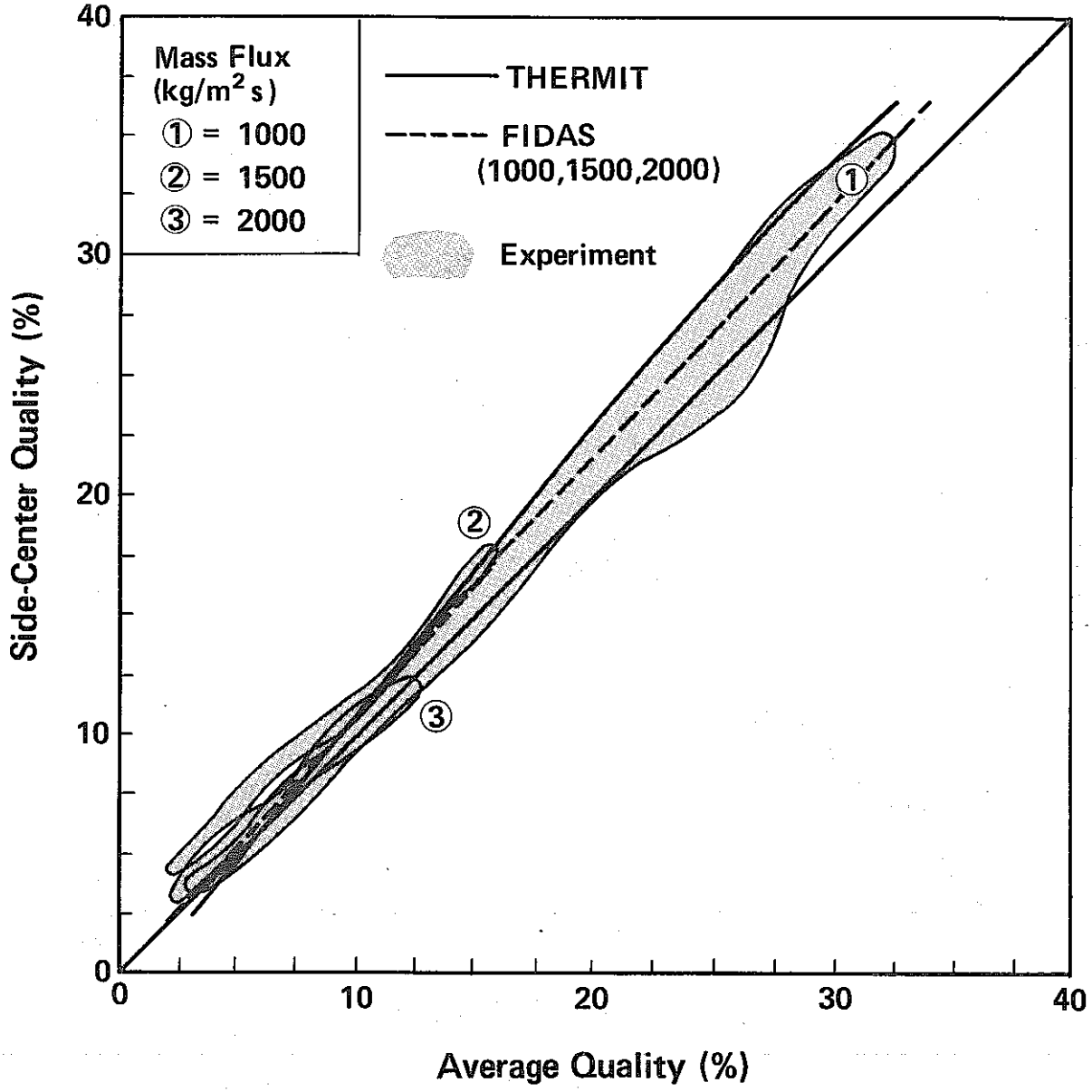

Fig. 13 Predicted and Measured Qualities for ISPRA-BWR Side-Center Subchannels

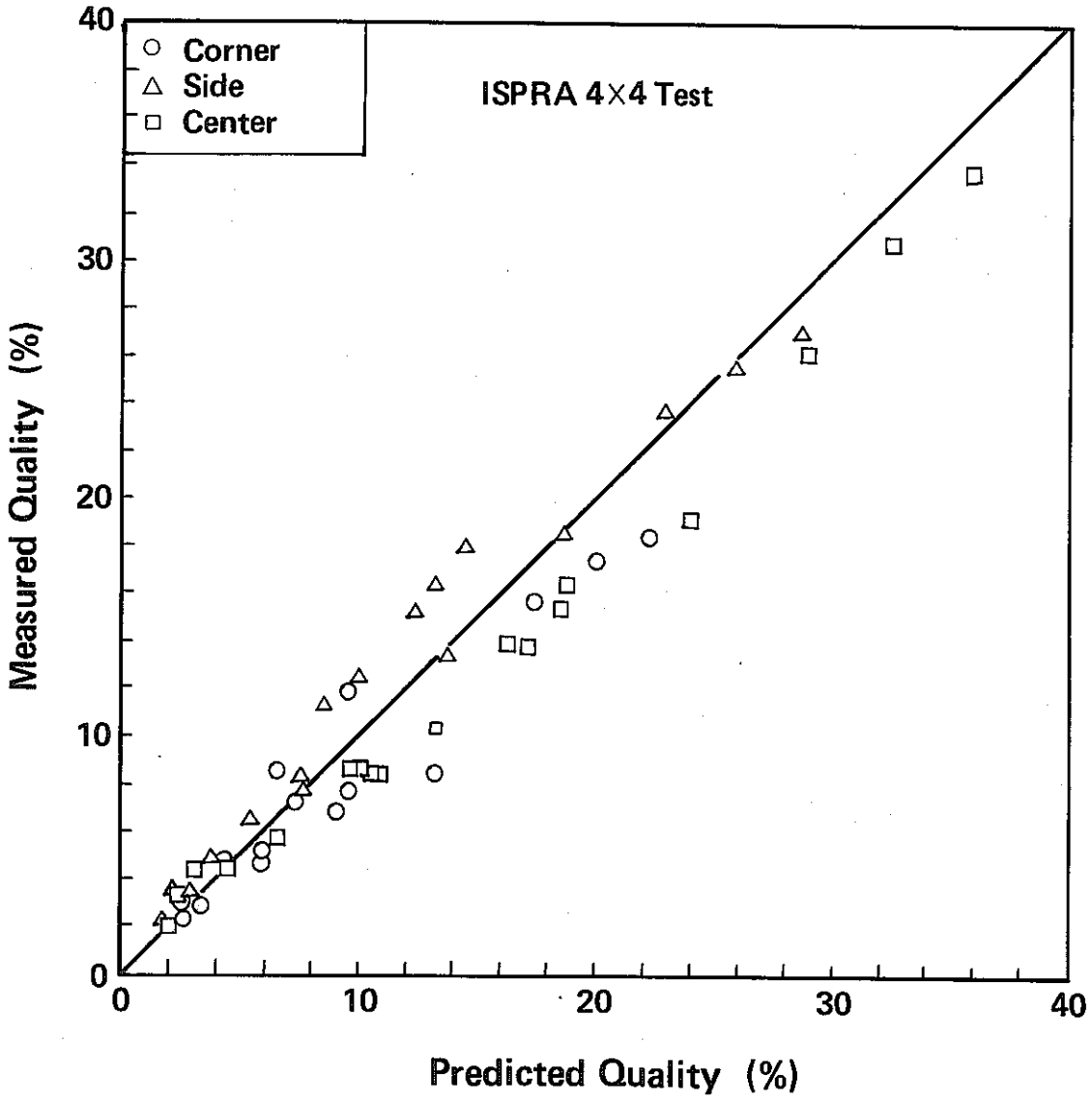

Fig. 14 Predicted and Measured Qualities for ISPRA-BWR Test

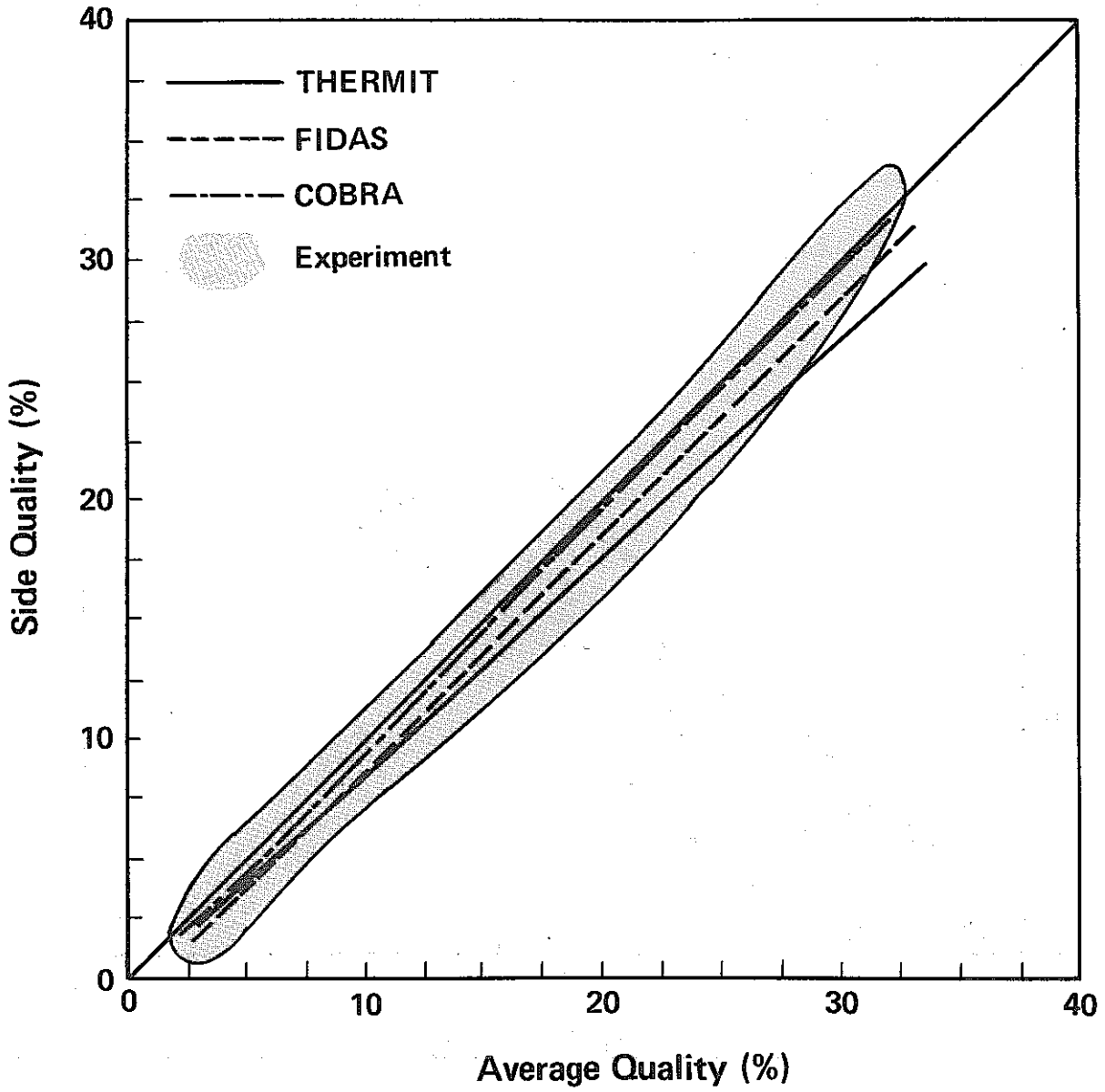

Fig. 15 Comparison of Predicted Qualities by Each Code with Measurement for GE Side Subchannel

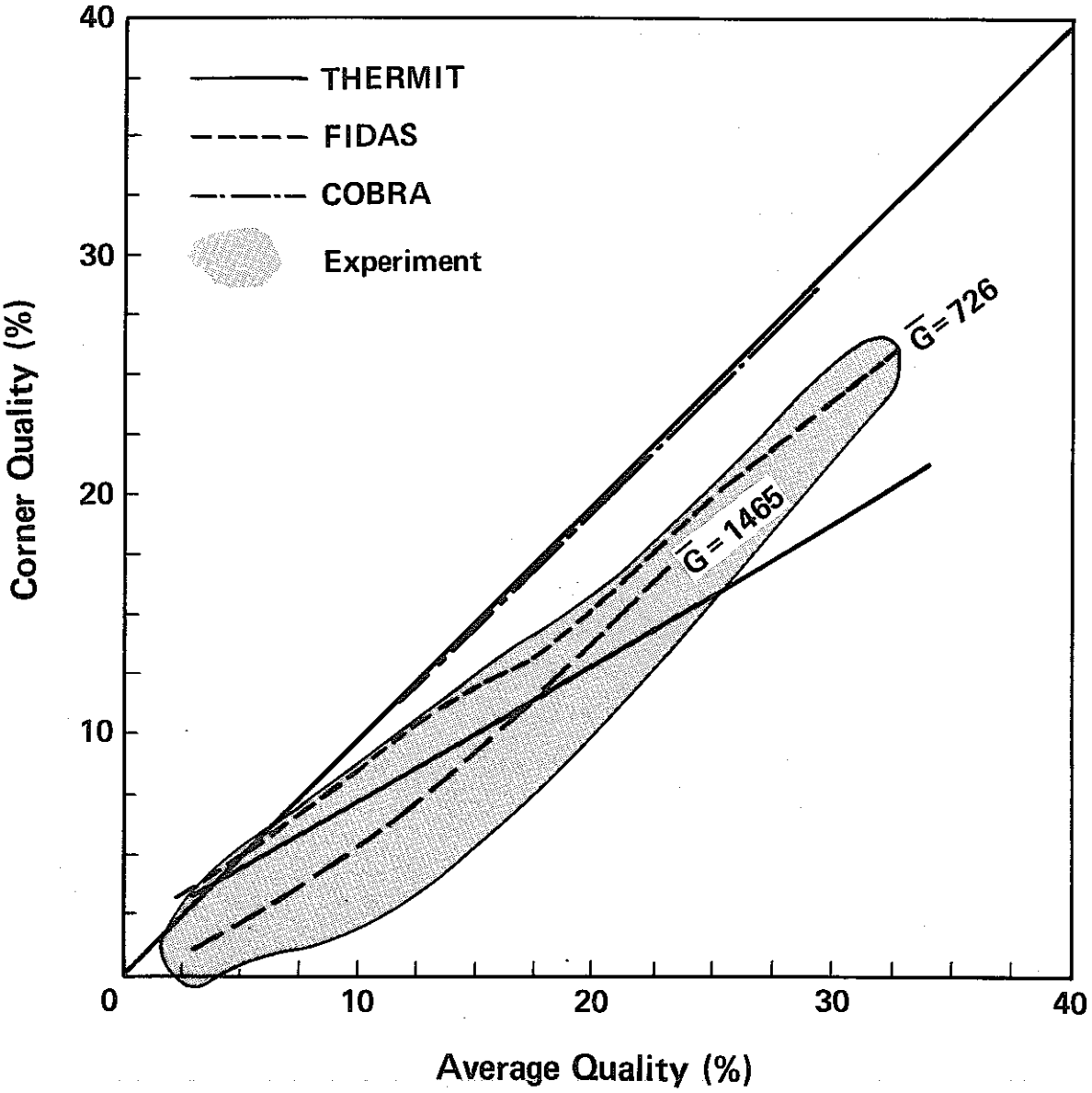

Fig. 16 Comparison of Predicted Qualities by Each Codes with Measurement for GE Corner Subchannel

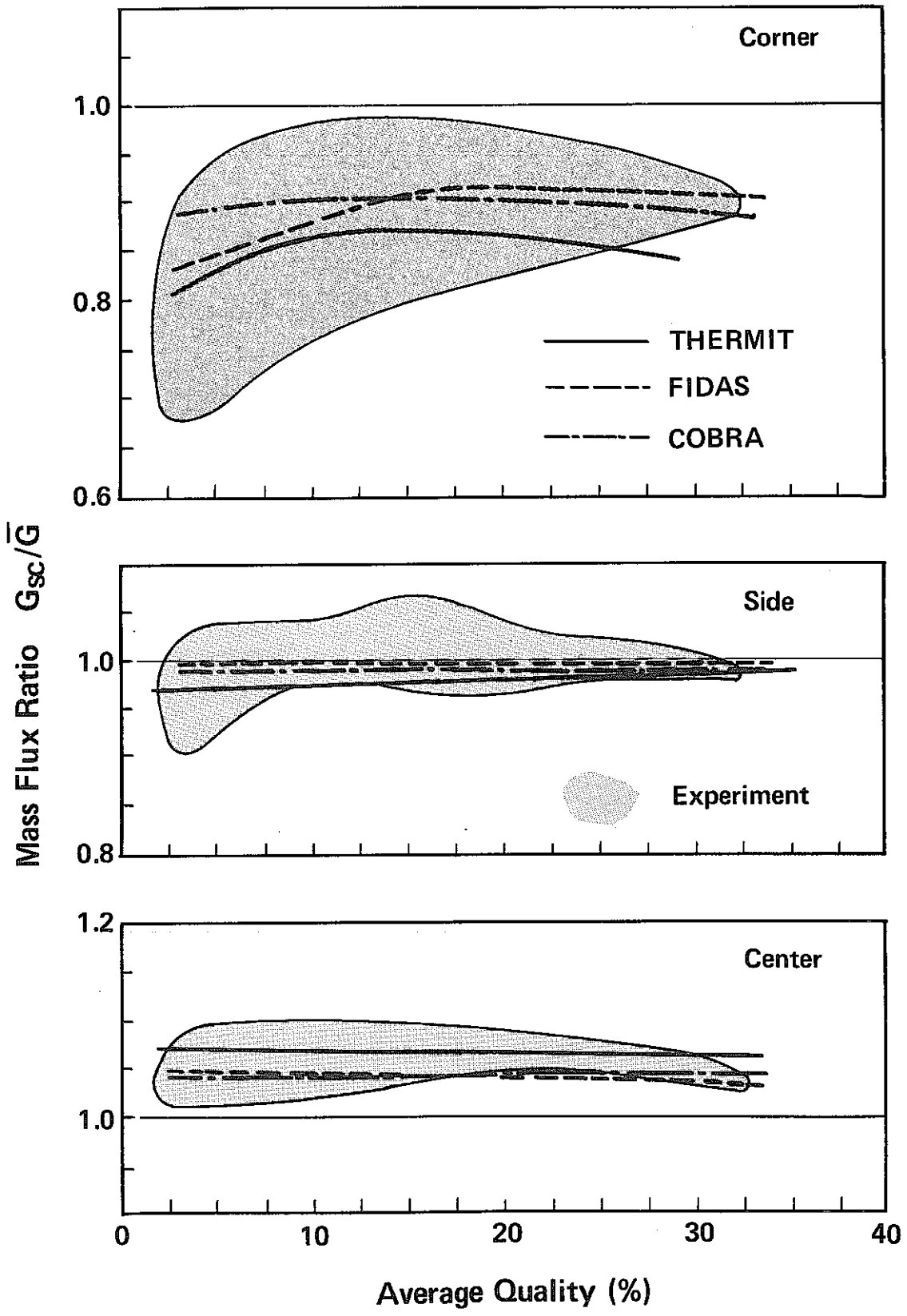

Fig. 17 Predicted and Measured Mass Flux Ratios for GE
(a) Corner (b) Side (c) Center Subchannels